



Article

# Multibeam Wideband Transmit Beamforming Using 2D Sparse FIR Trapezoidal Filters

Nadeeshan Dissanayake <sup>1</sup>, Chamira U. S. Edussooriya <sup>1,2</sup>, Chamith Wijenayake <sup>3</sup> and Arjuna Madanayake <sup>2,\*</sup>

<sup>1</sup> Department of Electronic and Telecommunication Engineering, University of Moratuwa, Moratuwa 10400, Sri Lanka; 160132l@uom.lk (N.D.); chamira@uom.lk (C.U.S.E.)

<sup>2</sup> Department of Electrical and Computer Engineering, Florida International University, Miami, FL 33199, USA

<sup>3</sup> School of Information Technology and Electrical Engineering, University of Queensland, Brisbane, QLD 4072, Australia; c.wijenayake@uq.edu.au

\* Correspondence: amadanay@fiu.edu

**Abstract:** A low-complexity multibeam wideband transmit beamformer using a 2D sparse FIR filter design capable of multiple beams is proposed as a digital building block for fully digital beamformers. The 2D sparse FIR filter has multiple trapezoid-shaped passbands pertaining to wideband beams aimed at particular directions. The proposed multibeam digital beamformer drives a uniform linear array of wideband antenna elements to achieve the wideband multibeam transmit-mode signals desired by the communication system. The 2D sparse FIR filter is designed to be optimal in the minimax sense using convex optimization techniques. Full-wave electromagnetic simulations using real antenna models confirm that the proposed wideband transmit beamformer can achieve multibeam transmission in the 1.3–2.8 GHz frequency range, with more than 70% fractional bandwidth. Furthermore, the adoption of the wideband transmit multibeam beamformer leads to a significant reduction in digital arithmetic (computational) complexity compared with previously reported wideband transmit beamformers of similar transfer function type, without deteriorating beam directionality and causing increases in the side-lobe level. The proposed sparse 2D FIR multibeam beamformer architecture is well-suited for both sub-6 GHz (legacy) band transmit beamforming, frequency range three (FR3) beamforming up to 28 GHz, and mmWave operation for emerging 5G/6G applications.

**Keywords:** transmit beamforming; multibeam; wideband; linear antenna arrays; 2D sparse FIR filters; minimax design



**Citation:** Dissanayake, N.; Edussooriya, C.U.S.; Wijenayake, C.; Madanayake, A. Multibeam Wideband Transmit Beamforming Using 2D Sparse FIR Trapezoidal Filters. *J. Low Power Electron. Appl.* **2024**, *14*, 26. <https://doi.org/10.3390/jlpea14020026>

Academic Editors: Stefania Perri and Costas Psychalinos

Received: 14 March 2024

Revised: 20 April 2024

Accepted: 23 April 2024

Published: 28 April 2024



**Copyright:** © 2024 by the authors. Licensee MDPI, Basel, Switzerland. This article is an open access article distributed under the terms and conditions of the Creative Commons Attribution (CC BY) license (<https://creativecommons.org/licenses/by/4.0/>).

## 1. Introduction

Directed electromagnetic energy is key in both radar and wireless communications [1–4]. The interferometric synthesis of a directed plane wave in the far-field using  $N$  independently driven radio-frequency (RF) emitters is known as “transmit beamforming” [5–9]. Modern wireless systems, such as 5G and emerging 6G millimeter Wave (mmWave) systems [3,10–12], utilize transmit beamformers at the access point. Furthermore, modern satellite transceivers [13–18] employ multibeam transmit beamformers to achieve wide-area coverage. Apertures consisting of antenna arrays with a large number of elements are to be expected, given that massive multi-input multi-output (MIMO) access is the dominant technology driving future wireless systems [1,3,19].

### 1.1. Multibeam Multichannel Access Points

In massive-MIMO arrays, the number of elements  $N$  can be orders of magnitude greater than the number of mutually independent wireless connections served by an access point. Further, access points having large apertures must connect to mobile units having both line of sight (LOS) and non-LOS RF propagation channels, in the presence of both short- and long-term fading. Non-LOS channels arise naturally due to the presence of large

reflectors in the environment. However, non-LOS channels are at times intentionally created by 6G systems using technologies such as large intelligent surfaces (LISs) and reconfigurable intelligent surfaces (RISs) [20–23]. Non-LOS channels may consist of multiple ray-like paths that bridge an access point to mobile units. Typically, the number of such dominant non-LOS paths takes small integer values (usually fewer than five) in number for many practical situations. Therefore, non-LOS channels require energy from the transmit power amplifiers to be spatially directed to multiple directions using  $M$  beams pointed at said directions, such that the best received signal-to-noise ratio (SNR) can be realized while imposing the lowest possible harmful interference to unintended receivers. A steerable multibeam multiuser transmit beamformer with capabilities for both channel equalization, adaptive interference control via spatial nulling, and rapid beam reconfiguration at low complexity is therein a rather crucial part of 5G/6G array processing systems.

### 1.2. Wideband vs. Narrowband Systems in Modern Applications

A beamformer may feed an antenna array with delays in a manner such that the transmitted waves interfere constructively in the far-field region along one or more desired directions. Destructive interference occurs along other directions, as determined by the zeros of the array factor polynomial, in order to achieve directional energy transmission and minimum harmful interference system wide. An aperture consisting of a number of uniformly spaced antennas driven by RF power amplifiers (PAs) enables a number of independent plane waves to be launched from a single array.

Assuming all of the transmit antennas are identical to each other, the far-field beam pattern is the product of the array factor and the element pattern of the antennas. Wideband beamforming refers to the situation when the bandwidth of interest is at least 10% of the center frequency of the operational band. The number of elements used in a transmit array determines the sharpness and angular accuracy of the beam. The sharpest possible beams are achieved when all of the beamforming weights are unity within the frequency band, leading to a rectangular windowing operation with known side-lobe levels of about  $-13.6$  dB for a large number of elements. Such beams are achieved using true-time delay beamformers. However, use cases in massive-MIMO for 5G/6G systems exist where multiple independent beams are required for illumination of different angular ranges by independent information-carrying signals. For serving non-LOS receivers, a single information-carrying signal needs to be directed to multiple directions with nulls placed at predetermined directions.

#### 1.2.1. Beam Sharpness vs. Degrees of Freedom

The sharpness of a given beam can be increased only by increasing the size of the physical aperture; the larger the number of antennas used, the larger the physical aperture, and thus the sharper the beams. Let the number of independent plane-waves that must be launched from an aperture be  $K$ . Then,  $K \leq N$ , where  $N$  is the number of elements used. When  $K = N$ , one obtains the maximum degrees of freedom, i.e., support for the maximum number of independent plane-waves from the array.

#### 1.2.2. RF–Analog Phasing vs. Fully Digital Schemes

There are several techniques for achieving multiple steerable and possibly independent RF transmit beams from an aperture containing  $N$  elements. Analog–RF, digital, and RF–analog—digital hybrid approaches [24,25] can be utilized for achieving wideband multibeam directed energy beamforming. In an analog–RF approach, as shown in Figure 1, signals corresponding to each independent plane-wave are applied to a digital-to-analog converter (DAC) and transmit chain, followed by a phase shifting and feed network before being applied to a PA that drives each antenna [6,8]. Note that each DAC output is bandpass filtered (BPF) and optionally upconverted to the carrier frequency, after which each channel is amplified and split into  $K$  outputs via an active or passive microwave splitter. The outputs of the power splitter are individually routed to  $N$  analog RF dot-product units, each having  $K$  phase-shifters and a  $K:1$  passive microwave combiner whose output is applied to the PA

of each of the antennas in the array. Furthermore, the  $N$  number of  $K$ -point dot-products is equivalent to a single RF–analog matrix–vector multiplication, where the input is a  $K$ -element vector, and the matrix is  $K \times N$ . Here, beamforming is achieved at RF using tunable delay lines. Wideband delays, however, are difficult to realize on integrated circuits making low size and weight integrated systems difficult to realize. Nevertheless, for narrowband systems, it is possible to realize tunable phase offsets for each PA input using programmable phasing circuits on chip. But the issue is that we need a dedicated set of phase-shifters for each independent beam, together with low-distortion microwave combiners and other associated electronics for signal combination prior to driving PA inputs.

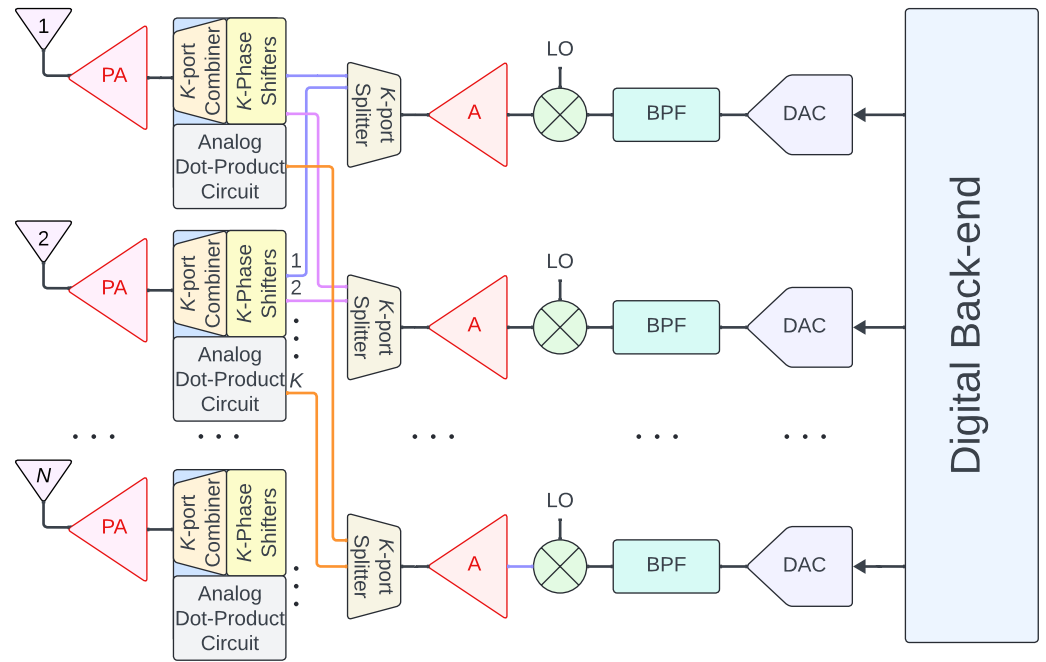


**Figure 1.** Conventional fully analog phasing matrices for achieving  $K$  beams: an  $N$ -element wideband antenna array is fed through  $N$  power amplifiers (PAs) using a digital intermediate frequency (IF) or baseband signal processor having  $N$  digital to analog converters (DACs).

### 1.3. Advantages of an All-Digital Approach

We can solve many such problems by adopting a fully digital transmit beamformer. In fully digital beamformers [26–28], beam personalities including main beams and null synthesis for each independent beam are achieved using discrete domain linear and time-invariant filtering methods implemented in real time on a fast digital signal processor (DSP). Multibeam combination is also achieved in the digital domain [29,30]. A dedicated DAC is used for each transmit chain driving the PAs so that maximum flexibility and reconfigurability are obtained.

### 1.4. Circuit Complexity vs. Flexibility

The overall circuit complexity and cost of such a solution is not scalable for even modest values of  $K$ . Fully digital approaches allow maximum flexibility on the number of independent beams, beam angles, beam sizes, and location of nulls. The PAs are directly driven by dedicated DACs at each antenna in the aperture, implying there is no need for RF–analog phase-shifters or true time-delay units to be used. Nevertheless, we note that fully digital approaches require up-link chains with the additional dynamic range due to the fact that  $K$  independent signals are multiplexed into the same  $N$  channels. Further, DAC resolution needs to increase by  $\log_2 K$  bits compared with the reference case where phasing and combining occur at the RF stage.

### 1.5. Fully Digital Wideband FIR Beamformers

Finite impulse response (FIR) filters can be used for transmit beamforming in a fully digital array. Wideband digital FIR realizations can be achieved with a set of narrowband FIR realizations, called sub-band beamformers, where a wideband signal is decomposed into a set of narrowband channels, and each channel is processed with complex-valued weight-and-sum feeding networks [6,31].

In [32], a low-complexity wideband transmit beamformer has been proposed using two-dimensional (2-D) sparse finite-extent impulse response (FIR) trapezoidal filters, designed using the windowing method and hard thresholding. This beamformer can achieve wideband operation with 33% fractional bandwidth and provides a path for lower computational complexity compared with comparable discrete Fourier transform (DFT)-based techniques. However, the FIR beamformer in [32] is limited to a single beam (i.e.,  $K = 1$ ), and the 2D sparse FIR trapezoidal filter is suboptimal because the windowing technique has been employed to design the filter. In the context of multibeam beamforming using FIR filters, one key limitation is computational complexity, especially for wideband systems with variously shaped passbands and narrow transition bands. The accuracy of the designed filters for each beam direction in a multibeam system is required to be high, leading to higher-order FIR filters with increased computational complexity. Achieving a wide passband for wideband operation can be challenging while maintaining a sharp transition band for side-lobe suppression. Our work addresses these limitations by designing a 2D sparse FIR trapezoidal filter to be optimal in the minimax sense for multibeam beamforming.

### 1.6. Proposed 2-D FIR Transmit Beamformer

We propose a fully digital transmit beamforming method based on 2-D sparse FIR trapezoidal filters and a uniform linear array (ULA) of wideband Vivaldi antennas [33], as shown in Figure 2. The proposed transmit beamformer is different from and improves on the standard FIR filter-and-sum transmit beamformers [34–36], where separate one-dimensional (1-D) FIR filters are employed for each antenna to implement the fractional time delays to achieve wideband operation. In particular, the proposed 2-D sparse FIR is optimal in the minimax sense and is designed using convex optimization techniques. Full-wave electromagnetic simulations using real antenna models confirm that the proposed wideband transmit beamformer can achieve multibeam transmission in the frequency range of 1.3–2.8 GHz, with more than 70% fractional bandwidth. Importantly, the proposed transmit beamformer provides considerable reduction in the computational complexity compared with nonsparse filter-and-sum transmit beamformers [34–36], 2-D nonsparse FIR filters [37–42], and 2-D sparse FIR filter [32], without deteriorating beam directionality and causing increases in the side-lobe level. Furthermore, the computational efficiency of our sparse FIR filter design makes them suitable for real-time beamforming applications in wideband systems, while the linear phase response within the passband of the filter contributes to maintaining signal fidelity during beam steering.

The proposed sparse 2-D FIR multibeam beamformer architecture is well-suited for both sub-6 GHz (legacy) band transmit beamforming, frequency range three (FR3) beamforming up to 28 GHz, as well as mmWave operation for emerging 5G/6G applications. Multibeam beamforming systems with sparse trapezoidal FIR filters offer several advantages, including flexibility in beam control, improved signal quality due to sharp transition bands, and the potential for real-time implementation with the sparse filter design. These advantages make them suitable for various applications. In the context of wireless communications, our work on multibeam beamforming could be beneficial for cellular networks to improve network capacity and user experience, especially in dense urban environments [43,44]. Additionally, for mmWave communication systems, the ability to form narrow beams with low side-lobes using 2D trapezoidal FIR filters is crucial for establishing high-data-rate links [29,30]. Multibeam beamforming allows radars to track multiple targets simultaneously or scan a wider area electronically [45–47]. Two-dimensional trapezoidal FIR filters can help shape the radar beam for specific applications like target tracking or

clutter suppression. We note that the underlying concepts are equally applicable for receive mode as well, even though we present only the transmit mode in this paper. Therefore, in remote sensing, multibeam systems can be used to acquire data from different observation angles [48,49]. Furthermore, 2D trapezoidal FIR filters can help achieve the desired beam patterns for specific features of interest in the scene.

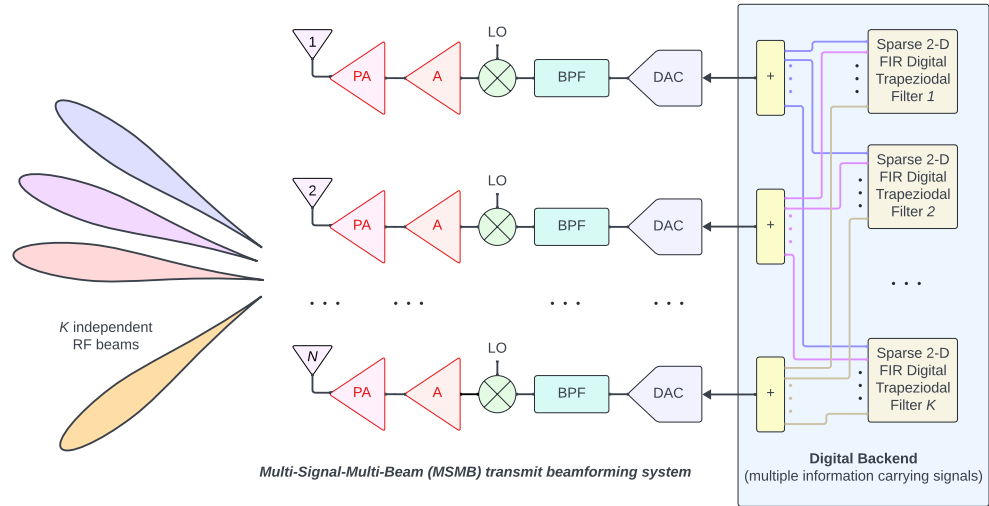


**Figure 2.** Architecture of the proposed transmit beamformer for the MSMB case, consisting of a filter bank of 2D sparse FIR trapezoidal filters, DACs, and RF front end, as well as a uniform linear array of broadband antennas.

## 2. Review of Spectra of 2D Plane Waves Received by Uniform Linear Arrays

We briefly review the spatiotemporal modeling of 2D plane waves received by a ULA and their spectra in this section. We consider the receive mode for the review because most of the related works on wideband beamforming using 2-D and three-dimensional filters consider receive-mode beamforming. A plane wave received by a ULA having  $N + 1$  wideband antennas placed along the  $x$  axis in the three-dimensional space  $(x, y, z) \in \mathbb{R}^3$  is shown in Figure 3a. Such a plane wave can be modeled as a 2-D discrete-domain spatiotemporal signal, after synchronous analog to digital conversion, which can be expressed as [50,51]

$$pw(n_x, n_{ct}) = w(\sin(\theta)n_x\Delta_x + n_{ct}\Delta_{ct}), \tag{1}$$

where  $(n_x, n_{ct}) \in \mathbb{Z}^2$ ,  $\theta$  (the zenith angle) denotes the direction of arrival (DOA) of the 2-D plane wave,  $\Delta_x$  and  $\Delta_{ct}$  are the sampling intervals in the  $x$  and  $ct$  domains, respectively,  $c$  is the constant speed of propagation of an electromagnetic wave, and  $w(n_{ct})$  specifies the 1-D temporal signal carried by the 2-D plane wave.

The ideal discrete-domain spectrum  $PW(\omega_x, \omega_{ct})$  of  $pw(n_x, n_{ct})$  can be obtained as [50,51]

$$PW(\omega_x, \omega_{ct}) = W(\omega_{ct})\delta(\omega_x - \sin(\theta)\omega_{ct}), \tag{2}$$

where  $(\omega_x, \omega_{ct}) \in \mathbb{R}^2$ ,  $\omega_{ct} = \omega_t/c$ ,  $W(\omega_{ct})$  is the spectrum of  $w(n_{ct})$ , and  $\delta(\cdot)$  is the 1-D continuous-domain impulse function. Note that  $\omega_x$  is the discrete-domain spatial frequency, and  $\omega_{ct}$  is the discrete-domain temporal frequency scaled by  $c$ . The region of support (ROS)  $\mathcal{R}$  of  $PW(\omega_x, \omega_{ct})$  can be obtained as [50,51]

$$\mathcal{R} = \{(\Omega_x, \Omega_{ct}) \in \mathbb{R}^2 | (\Omega_x - \sin(\theta)\Omega_{ct}) = 0, W(\Omega_{ct}) \neq 0\}, \tag{3}$$

which lies on a straight line going through the origin of the 2-D discrete frequency domain, as shown in Figure 3b. The angle  $\alpha$  between the ROS of the plane wave and the  $\omega_{ct}$  axis is given by [39,50]

$$\alpha = \tan^{-1}(\sin(\theta)). \tag{4}$$

In the case of  $K \in \mathbb{Z}^+$  plane waves having different DOAs  $\theta_k$  and  $w_k(ct)$ ,  $k = 1, 2, \dots, K$ , received by a ULA, the *ideal* discrete-domain spectrum  $PW_K(\omega_x, \omega_{ct})$  is given by

$$PW_K(\omega_x, \omega_{ct}) = \sum_{k=1}^K W_k(\omega_{ct}) \delta(\omega_x - \sin(\theta_k)\omega_{ct}). \tag{5}$$

In this case, the spectral ROS  $\mathcal{R}_K$  lies on  $K$  straight lines going through the origin inside the principal Nyquist square of the 2-D discrete frequency domain with  $\alpha_k = \tan^{-1}(\sin(\theta_k))$ . In practice, the true ROS of the generated discrete-domain 2-D plane wave is a narrow parallelogram when the number of antennas is finite. In the case of a 2-D *broadband bandpass* plane wave having a temporal bandwidth  $B_{ct}$  with center frequency  $\Omega_{ct}^c$ , as shown in the Figure 4, the desired 2-D plane wave (PW) (signal of interest) can be extracted by using a 2D filter having *narrow-angle double-trapezoidal-shaped passbands* [39,40]. This will attenuate noise and radio frequency interference (RFI) having DOAs that are different from the DOA of the signal of interest.

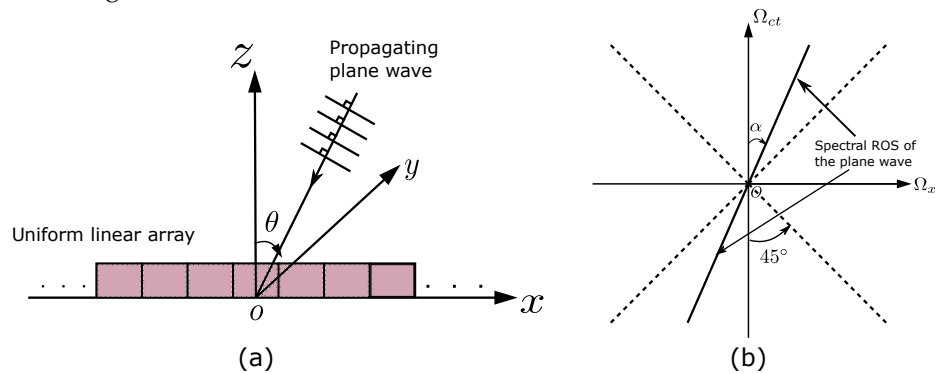


**Figure 3.** (a) Propagating PW received by an ULA situated on the  $x$  axis, (b) ROS of  $PW_{2C}(\Omega_x, \Omega_{ct})$ . Note that the angle  $|\theta| \leq 90^\circ$  leads to  $|\alpha| \leq 45^\circ$ .

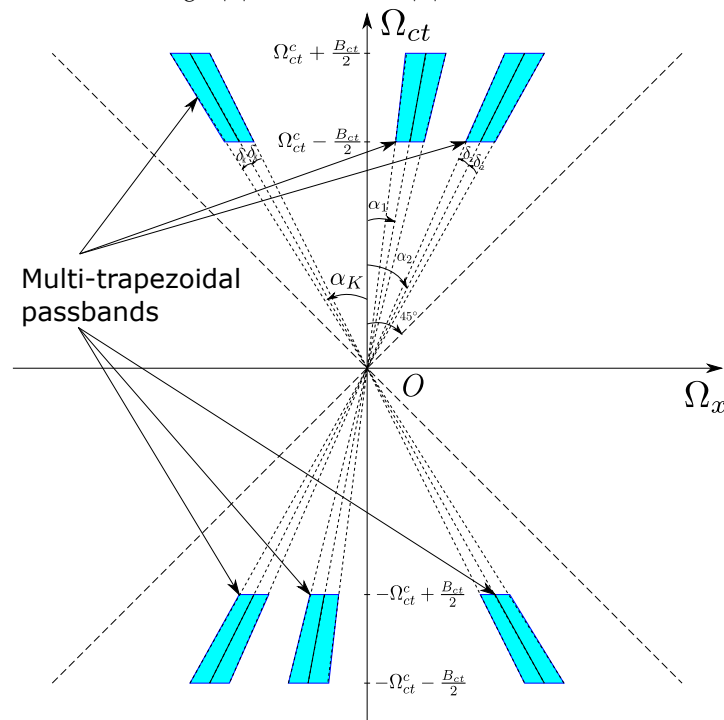


**Figure 4.** Spectral ROS of broadband bandpass 2D plane wave having different DOAs or DODs, as well as multiple trapezoidal passbands of the 2D FIR filter.

The same analysis can be applied to the transmit beamforming, where 2-D wideband plane waves are emitted by a ULA in  $K$  different directions, i.e, with direction of departures

(DODs)  $\theta_k; k = 1, 2, \dots, K$ . In this case, the spectral ROS of the required 2-D digital filter should consist of  $K$  narrow-angle double-trapezoidal-shaped passbands, as shown in Figure 4. In our proposed system, we use 2-D sparse FIR filters with trapezoidal passbands, as shown in Figure 4. A single trapezoidal passband is specified by the temporal bandwidth of the broadband bandpass plane wave, as well as the angle  $\alpha_k; k = 1, 2, \dots, K$  which depends on the DOD and the half-angle  $\delta_k$ . The operation of the multibeam transmit beamformer is explained in detail in the next section.

### 3. Proposed Low-Complexity Multibeam Wideband Transmit Beamformer

In this section, we present the proposed multibeam wideband beamformer in detail. To this end, we first present an overview of the architecture of the proposed multibeam wideband beamformer.

#### 3.1. Proposed Sparse 2D FIR Multibeam Beamformer

The proposed transmit beamformer comprises a 2-D sparse FIR filter or a filter bank, DACs, RF front-end including power amplifiers (PAs), and a ULA of broadband antennas, as shown in Figure 2. The proposed transmit beamformer is fully digital and supports for  $K \leq N$  independently steerable wideband beams in two modes: 1) one wideband signal is transmitted in  $K$  independent directions (denoted as single-signal multi-beam (SSMB)) and 2)  $K$  independent wideband signals are transmitted in  $K$  independent directions (denoted as multi-signal multi-beam (MSMB)). For the SSMB case, we employ a 2-D sparse FIR filter having  $K$  trapezoidal passbands, and for the MSMB case, we employ a filter bank consisting of 2-D sparse FIR filters having single trapezoidal passband. Trapezoidal passbands are chosen because of their constant half-angle  $\delta_k$  throughout the passbands, as shown in Figure 4. This enables the multibeam beamformer to generate constant beamwidth in the main lobes throughout the wideband frequency range. We note that, in the MSMB case, a dedicated 2-D sparse FIR filter is used for each independent far-field plane-wave corresponding to an independent information-carrying signal with a digital combination of plane-wave components after the filter bank, allowing a single set of DACs and RF chain to support  $K$  independent beams using the ULA.

In order to explain the operation of the transmit beamformer, we consider the SSMB case, where the 1-D signal  $w(n_{ct}), n_{ct} \in \mathbb{Z}$  is required to transmit in the  $K$  directions  $\theta_1, \theta_2, \dots, \theta_K$ . We call  $\theta_i (\in [-90^\circ, 90^\circ], i = 1, 2, \dots, K)$  as the DODs. Here, broadband antennas are fed with the 2-D mixed-domain signal  $s_m(n_x \Delta_x, ct)$ , where  $(n_x, ct) \in \mathbb{Z} \times \mathbb{R}$ , which consists of appropriately scaled and delayed continuous-time counterparts of  $w(n_{ct})$  in order to achieve transmit beamforming. Note that the electromagnetic waves emanating from broadband antennas constructively interfere in the far field to form a beam pattern with  $K$  beams along the directions of  $\theta_1, \theta_2, \dots, \theta_K$ . The 2-D sparse FIR filter  $H(z_x, z_{ct})$  with  $K$  trapezoidal passbands is employed to scale and delay  $w(n_{ct})$  appropriately to realize  $K$  beams, where the  $i$ th ( $= 1, 2, \dots, K$ ) trapezoidal passband provides the scaled and delayed  $w(n_{ct})$  for the  $i$ th beam. This is analogous to the use of a 2-D filter with  $K$  trapezoidal passbands to realize  $K$  beams in the receive mode beamforming, as reviewed in Section 2. The DACs and the PAs in the RF chains are used for the discrete-time to continuous-time conversion and to realize the required power gain, respectively.

Now, let us consider the processing of the 2-D sparse FIR filter. The 2-D discrete-domain input signal  $s_{in}(n_x, n_{ct}), (n_x, n_{ct}) \in \mathbb{Z}^2$  of  $H(z_x, z_{ct})$  is defined as

$$s_{in}(n_x, n_{ct}) = \begin{cases} w(n_{ct}), & n_x = 0 \\ 0, & \text{otherwise.} \end{cases} \quad (6)$$

$H(z_x, z_{ct})$  should have trapezoidal-shaped passbands in the principal Nyquist square  $\mathcal{N}$  of the 2-D discrete frequency domain  $(\omega_x, \omega_{ct}) \in \mathbb{R}^2$ , as shown in Figure 4, to achieve the required scaled and delayed versions of the wideband input signal  $w(n_{ct})$ , in the 2-D

discrete-domain output signal  $s_{out}(n_x, n_{ct})$  of the digital filter. Here,  $\mathcal{N} = \{(\omega_x, \omega_{ct}) \in \mathbb{R}^2, -\pi \leq \omega_x, \omega_{ct} < \pi\}$ . The output signal  $s_{out}(n_x, n_{ct})$  is given by

$$s_{out}(n_x, n_{ct}) = \sum_{(i_x, i_{ct}) \in \mathcal{I}} h_s(i_x, i_{ct}) s_{in}(n_x - i_x, n_{ct} - i_{ct}) \quad (7)$$

where  $\mathcal{I}$  is the set containing the indices of the nonzero coefficients of the impulse response  $h_s(i_x, i_{ct})$  of  $H(z_x, z_{ct})$ . Here,  $s_{out}(n_x, n_{ct})$  is computed for  $-(N_x-1)/2 \leq n_x \leq (N_x-1)/2$  and  $0 \leq n_{ct} \leq (N_{ct} - 1)$ , where  $N_x$  and  $N_{ct}$  are the number of broadband antennas in the ULA and the number of temporal samples in  $w(n_{ct})$ , respectively. The design of  $H(z_x, z_{ct})$  with sparse coefficients is presented next.

### 3.2. Two-Dimensional Sparse FIR Trapezoidal Filter

The 2-D sparse FIR trapezoidal filter  $H(z_x, z_{ct})$  is designed by using the FIR filter design method presented in [52]. To this end, the required passband  $\mathcal{R}_{PB}$  of the 2D filter  $H(z_x, z_{ct})$  having  $K$  double trapezoidal passbands inside the principal Nyquist square  $\mathcal{N}$  can be derived as

$$\mathcal{R}_{PB} = \bigcup_{k=1}^K \mathcal{R}_k \quad (8)$$

where  $\mathcal{R}_k$  is the trapezoidal passband corresponding to the  $k$ th bandpass 2-D PW, which is given by

$$\begin{aligned} \mathcal{R}_k = \left\{ (\omega_x, \omega_{ct}) \in \mathcal{N} \mid \left[ \Omega_{ct}^{C_k} - \frac{B_{ct}^k}{2} \geq |\omega_{ct}| \geq \Omega_{ct}^{C_k} + \frac{B_{ct}^k}{2} \right] \right. \\ \left. \cap \left[ (\omega_x \leq \tan(\alpha_k + \delta_k) \omega_{ct} \cap \omega_x \geq \tan(\alpha_k - \delta_k) \omega_{ct}) \right. \right. \\ \left. \left. \cup (\omega_x \geq \tan(\alpha_k + \delta_k) \omega_{ct} \cap \omega_x \leq \tan(\alpha_k - \delta_k) \omega_{ct}) \right] \right\}, \quad (9) \end{aligned}$$

where  $B_{ct}^k$  is the temporal bandwidth of the  $k$ th PW,  $\Omega_{ct}^{C_k}$  is the center frequency of the  $k$ th PW, and  $\delta_k$  is the half-angle of the double trapezoidal-shaped  $k$ th passband. The value of  $\delta_k$  affects the beamwidth of the multibeams produced by the transmit beamformer.

The ideal frequency response  $H_d(e^{j\omega_x}, e^{j\omega_{ct}})$  of  $H(z_x, z_{ct})$  inside  $\mathcal{N}$  is specified as

$$H_d(e^{j\omega_x}, e^{j\omega_{ct}}) = \begin{cases} 1, & (\omega_x, \omega_{ct}) \in \mathcal{R}_{PB} \\ 0, & \text{otherwise.} \end{cases} \quad (10)$$

Note that  $H_d(e^{j\omega_x}, e^{j\omega_{ct}})$  has a zero group delay with respect to both  $\omega_x$  and  $\omega_{ct}$ .

### 3.3. Minimax Design of the 2D Sparse FIR Filter

The design of  $H(z_x, z_{ct})$  is presented in this subsection, adapting the 2-D sparse FIR filter design method proposed in [52]. We choose the filter design method in the minimax sense to reduce the side-lobe levels. To this end, we express the frequency response of  $H(z_x, z_{ct})$  as

$$H(e^{j\omega_x}, e^{j\omega_{ct}}) = \sum_{n_x = -\frac{N_x}{2}}^{\frac{N_x}{2}} \sum_{n_c = -\frac{N_c}{2}}^{\frac{N_c}{2}} h(n_x, n_c) e^{-j(n_x \omega_x + n_c \omega_{ct})}, \quad (11)$$

where  $h(n_x, n_c)$  is the impulse response of size  $(N_x + 1) \times (N_c + 1)$  (order =  $N_x \times N_c$ ). The order of the filter depends on the number of broadband antennas in the ULA and the expected accuracy of the beams produced by the transmit beamformer.  $H(z_x, z_{ct})$  is designed as a zero-phase filter ([53], Chapter 3). The impulse response of the filter is

centrosymmetric in this case, i.e.,  $h(n_x, n_c) = h(-n_x, -n_c)$ . Therefore, considering the centrosymmetric property,  $H(e^{j\omega_x}, e^{j\omega_{ct}})$  can be simplified as

$$H(e^{j\omega_x}, e^{j\omega_{ct}}) = h(0, 0) + \sum_{n_x=1}^{\frac{N_x}{2}} 2h(n_x, 0) \cos(n_x \omega_x) + \sum_{n_x=-\frac{N_x}{2}}^{\frac{N_x}{2}} \sum_{n_c=1}^{\frac{N_c}{2}} 2h(n_x, n_c) \cos(n_x \omega_x + n_c \omega_{ct}), \tag{12}$$

which is represented in vector form by

$$H(e^{j\omega_x}, e^{j\omega_{ct}}) = \mathbf{c}(\omega_x, \omega_{ct})^T \mathbf{h}. \tag{13}$$

where,

$$\mathbf{h} = \left[ h(0, 0), 2h(1, 0), \dots, 2h\left(\frac{N_x}{2}, 0\right), 2h\left(\frac{-N_x}{2}, 1\right), \dots, 2h\left(\frac{N_x}{2}, \frac{N_c}{2}\right) \right]^T, \tag{14}$$

and

$$\mathbf{c}(\omega_x, \omega_{ct}) = \left[ 1, \cos(\omega_x), \dots, \cos\left(\frac{N_x}{2} \omega_x\right), \cos\left(\frac{-N_x}{2} \omega_x + \omega_{ct}\right), \dots, \cos\left(\frac{N_x}{2} \omega_x + \frac{N_c}{2} \omega_{ct}\right) \right]^T. \tag{15}$$

In [52], a two-phase design method for 2D FIR digital filters in weighted minimax design applicable for filters having quadrantly symmetric impulse responses was presented. With (13), this approach can be used to design  $H(z_x, z_{ct})$  despite its centro-symmetric impulse response.

### 3.3.1. Step 1

We obtain an intermediate sparse impulse response in the weighted minimax sense. The objective function to be minimized is expressed as

$$\underset{\mathbf{h}}{\text{minimize}} \left[ \max_{(\omega_x, \omega_{ct}) \in \mathcal{F}} W(\omega_x, \omega_{ct}) |H(e^{j\omega_x}, e^{j\omega_{ct}}) - H_d(e^{j\omega_x}, e^{j\omega_{ct}})| + \mu \|\mathbf{h}\|_1 \right] \tag{16}$$

where  $H(e^{j\omega_x}, e^{j\omega_{ct}})$  is given in (13),  $H_d(e^{j\omega_x}, e^{j\omega_{ct}})$  is given in (10), and  $W(\omega_x, \omega_{ct})$  is a weighting function used to control the passband ripple and stopband ripple, which affects the side-lobes of the transmit beamformer across the bandwidth. Parameter  $\mu$  is a small positive number (typically between 0.001 and 1 [54]), and  $\mathcal{F}$  is the region corresponding to the passband and stopband, i.e., without the transition band [52]. Due to the centrosymmetric impulse response of  $H(e^{j\omega_x}, e^{j\omega_{ct}})$ , only the region  $[-\pi, \pi] \times [0, \pi]$  in the 2-D frequency domain  $(\omega_x, \omega_{ct})$  is considered to define  $\mathcal{F}$ . By introducing an upper bound  $\beta$  for  $W(\omega_x, \omega_{ct}) |H(e^{j\omega_x}, e^{j\omega_{ct}}) - H_d(e^{j\omega_x}, e^{j\omega_{ct}})|$  over a finite  $M$  set of frequency grids  $\Omega_d = \{\omega_i = (\omega_1^{(i)}, \omega_2^{(i)}), 1 \leq i \leq M\} \subseteq \mathcal{F}$ , (16) is reduced to a tractable constrained problem as

$$\text{minimize } \beta + \mu \|\mathbf{h}\|_1$$

$$\begin{aligned} \text{subject to : } & W(\omega_i)|H(e^{j\omega_1^{(i)}}, e^{j\omega_2^{(i)}}) - \\ & H_d(e^{j\omega_1^{(i)}}, e^{j\omega_2^{(i)}})| \leq \beta, 1 \leq i \leq M \end{aligned} \tag{17}$$

To deal with the nondifferentiability of  $\|\mathbf{h}\|_1$ , taking an upper bound for each entry of  $\mathbf{h}$ , i.e.,

$$|h_i| \leq d_i \text{ for } 1 \leq i \leq n \tag{18}$$

with  $n = 1 + \frac{N_x + N_x N_c + N_c}{2}$ , leads (17) to

$$\begin{aligned} \text{minimize } & \beta + \mu \sum_{i=1}^n d_i \\ \text{subject to : } & W(\omega_i)|\mathbf{c}(\omega_i)^T \mathbf{h} - \\ & H_d(e^{j\omega_1^{(i)}}, e^{j\omega_2^{(i)}})| \leq \beta \text{ for } 1 \leq i \leq M \\ & |h_i| \leq d_i \text{ for } 1 \leq i \leq n \end{aligned} \tag{19}$$

Treating the bounds  $\beta$  and  $d_i (1 \leq i \leq n)$  as auxiliary design variables in (19), the optimization problem becomes a convex optimization problem, which can be converted as a linear programming (LP) problem [52] expressed as

$$\begin{aligned} \text{minimize } & \mathbf{f}^T \mathbf{x} \\ \text{subject to : } & \mathbf{A} \mathbf{x} \geq \mathbf{b} \end{aligned} \tag{20}$$

where

$$\begin{aligned} \mathbf{d} = \begin{bmatrix} d_1 \\ d_2 \\ \vdots \\ d_n \end{bmatrix}, \mathbf{h} = \begin{bmatrix} h_1 \\ h_2 \\ \vdots \\ h_n \end{bmatrix}, \mathbf{e}_n = \begin{bmatrix} 1 \\ 1 \\ \vdots \\ 1 \end{bmatrix}_{n \times 1}, \mathbf{x} = \begin{bmatrix} \beta \\ \mathbf{d} \\ \mathbf{h} \end{bmatrix}, \\ \mathbf{f} = \begin{bmatrix} 1 \\ \mu \mathbf{e}_n \\ \mathbf{0} \end{bmatrix}, \mathbf{A} = \begin{bmatrix} \mathbf{A}_1 \\ \mathbf{A}_2 \end{bmatrix}, \mathbf{b} = \begin{bmatrix} \mathbf{b}_1 \\ \mathbf{0} \end{bmatrix}, \end{aligned} \tag{21}$$

with

$$\begin{aligned} \mathbf{A}_1 = \begin{bmatrix} 1 & \mathbf{0} & W(\omega_1)\mathbf{c}^T(\omega_1) \\ \vdots & \vdots & \vdots \\ 1 & \mathbf{0} & W(\omega_M)\mathbf{c}^T(\omega_M) \\ 1 & \mathbf{0} & -W(\omega_1)\mathbf{c}^T(\omega_1) \\ \vdots & \vdots & \vdots \\ 1 & \mathbf{0} & -W(\omega_M)\mathbf{c}^T(\omega_M) \end{bmatrix}, \mathbf{A}_2 = \begin{bmatrix} \mathbf{0} & \mathbf{I}_n & \mathbf{I}_n \\ \mathbf{0} & \mathbf{I}_n & -\mathbf{I}_n \end{bmatrix}, \\ \mathbf{b}_1 = \begin{bmatrix} W(\omega_1)H_d(e^{j\omega_1^{(1)}}, e^{j\omega_2^{(1)}}) \\ \vdots \\ W(\omega_M)H_d(e^{j\omega_1^{(M)}}, e^{j\omega_2^{(M)}}) \\ -W(\omega_1)H_d(e^{j\omega_1^{(1)}}, e^{j\omega_2^{(1)}}) \\ \vdots \\ -W(\omega_M)H_d(e^{j\omega_1^{(M)}}, e^{j\omega_2^{(M)}}) \end{bmatrix} \end{aligned} \tag{22}$$

The unique and globally optimal solution  $\mathbf{h}$  of the linear programming problem is an approximately sparse [52]. To obtain a sparse impulse response  $\mathbf{h}^s$ , hard thresholding is employed, i.e.,

$$h_i^s = \begin{cases} h_i, & \text{if } |h_i| \geq \epsilon_{th} \\ 0, & \text{otherwise,} \end{cases} \quad (23)$$

where  $\epsilon_{th} (\in [10^{-4}, 10^{-2}])$  typically [54] is the threshold value.

### 3.3.2. Step 2

We again optimize  $\mathbf{h}^s$  in the weighted minimax sense in order to obtain the optimal solution for the 2-D sparse FIR filter. This optimization problem is expressed as

$$\begin{aligned} & \underset{\mathbf{h}^s}{\text{minimize}} \left[ \max_{(\omega_x, \omega_{ct}) \in \mathcal{F}} W(\omega_x, \omega_{ct}) |\mathbf{c}(\omega_x, \omega_{ct})^T \mathbf{h}^s \right. \\ & \qquad \qquad \qquad \left. - H_d(e^{j\omega_x}, e^{j\omega_{ct}}) \right] \\ & \text{subject to : } h_i^s = 0 \text{ for } i \in I_\infty, \end{aligned} \quad (24)$$

where  $I_\infty$  is the set containing indices  $i$  for which  $h_i^s = 0$ . Again, by introducing an upper bound  $\beta$  for  $W(\omega_x, \omega_{ct}) |\mathbf{c}(\omega_x, \omega_{ct})^T \mathbf{h}^s - H_d(e^{j\omega_x}, e^{j\omega_{ct}})|$  over a finite  $M$  set of frequency grids  $\Omega_d = \{\omega_i = (\omega_1^{(i)}, \omega_2^{(i)}), 1 \leq i \leq M\} \subseteq \mathcal{F}$ , (24) is reduced to a tractable constrained problem as

$$\begin{aligned} & \text{minimize } \beta \\ & \text{subject to : } W(\omega_i) |\mathbf{c}(\omega_i)^T \mathbf{h}^s - \\ & \qquad \qquad \qquad H_d(e^{j\omega_1^{(i)}}, e^{j\omega_2^{(i)}})| \leq \beta \text{ for } 1 \leq i \leq M \\ & \qquad \qquad \qquad h_i^s = 0 \text{ for } i \in I_\infty, \end{aligned} \quad (25)$$

By defining vectors  $\hat{\mathbf{h}}^s$  and  $\hat{\mathbf{c}}(\omega)$  by deleting those entries of  $\mathbf{h}^s$  and  $\mathbf{c}(\omega)$  whose indices belong to set  $I_\infty$ , we have  $\mathbf{c}(\omega)^T \mathbf{h}^s = \hat{\mathbf{c}}(\omega)^T \hat{\mathbf{h}}^s$ . Hence, (25) can be written as

$$\begin{aligned} & \text{minimize } \beta \\ & \text{subject to : } W(\omega_i) |\hat{\mathbf{c}}(\omega_i)^T \hat{\mathbf{h}}^s - \\ & \qquad \qquad \qquad H_d(e^{j\omega_1^{(i)}}, e^{j\omega_2^{(i)}})| \leq \beta \text{ for } 1 \leq i \leq M \end{aligned} \quad (26)$$

With  $\beta$  as an auxiliary variable, problem (26) becomes an LP problem of the form

$$\begin{aligned} & \text{minimize } \mathbf{f}^T \mathbf{x} \\ & \text{subject to : } \mathbf{A} \mathbf{x} \geq \mathbf{b} \end{aligned} \quad (27)$$

where

$$\mathbf{x} = \begin{bmatrix} \beta \\ \hat{\mathbf{h}} \end{bmatrix}, \mathbf{f} = \begin{bmatrix} 1 \\ \mathbf{0} \end{bmatrix}, \mathbf{A} = \begin{bmatrix} 1 & W(\omega_1) \hat{\mathbf{c}}^T(\omega_1) \\ \vdots & \vdots \\ 1 & W(\omega_M) \hat{\mathbf{c}}^T(\omega_M) \\ 1 & -W(\omega_1) \hat{\mathbf{c}}^T(\omega_1) \\ \vdots & \vdots \\ 1 & -W(\omega_M) \hat{\mathbf{c}}^T(\omega_M) \end{bmatrix},$$

$$\mathbf{b} = \begin{bmatrix} W(\omega_1)H_d(e^{j\omega_1^{(1)}}, e^{j\omega_2^{(1)}}) \\ \vdots \\ W(\omega_M)H_d(e^{j\omega_1^{(M)}}, e^{j\omega_2^{(M)}}) \\ -W(\omega_1)H_d(e^{j\omega_1^{(1)}}, e^{j\omega_2^{(1)}}) \\ \vdots \\ -W(\omega_M)H_d(e^{j\omega_1^{(M)}}, e^{j\omega_2^{(M)}}) \end{bmatrix}.$$

By solving (27), the impulse response of the required 2-D FIR filter  $\mathbf{h}^s$  can be obtained.

### 3.4. Analysis and Selection of Parameters

Finding an optimal balance between the performance and the computational complexity of the sparse FIR filter is a challenge. When solving the optimization problem in the design of the filter, the parameters  $\mu$  and  $\epsilon_{th}$  were chosen such that the sparsity of the filter impulse response was significant without substantially degrading the filter performance. For a particular filter design, the value for the parameter  $\mu$  is varied in the range [0.001, 1], fixing the number of nonzero values in the impulse response, and the filter performance is observed in terms of the optimal value of step 2 of the optimization problem, which is the weighted maximum error between the desired response and the actual response,  $E_{opt}$ . The value that gave the best performance out of the tested values is chosen for the design of the particular filter. After choosing a suitable value for  $\mu$ , to choose a suitable threshold  $\epsilon_{th}$ , the root-mean-square-error (RMSE)  $E$ , and  $E_{opt}$ , are considered.  $E$  is given by

$$E = \sqrt{\sum_{i=1}^M \frac{(|H(e^{j\omega_1^{(i)}}), e^{j\omega_2^{(i)}})| - |H_d(e^{j\omega_1^{(i)}}), e^{j\omega_2^{(i)}})|)^2}{M}} \tag{28}$$

When the number of nonzero coefficients is decreased by using a suitable  $\epsilon_{th}$ , the  $E_{opt}$  increases rapidly after some point, as shown in Figure 5. Therefore,  $\epsilon_{th}$  is chosen such that it yields the required number of nonzero values without increasing the  $E_{opt}$  substantially. As a rule of thumb,  $\epsilon_{th}$  is chosen such that  $E_{opt}$  does not exceed more than 0.05 of its initial value and  $E < 10\%$ .

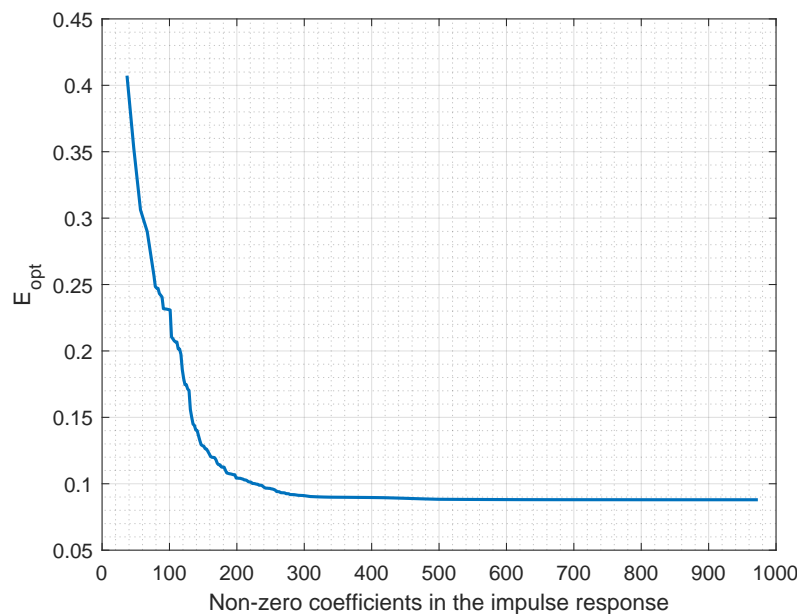


**Figure 5.**  $E_{opt}$  variation with the number of nonzero values in the impulse response of the proposed 2-D FIR trapezoidal filter.

As an example, Figure 5 shows the variation in  $E_{opt}$  vs. the nonzero values in the impulse response for the case of the single-beam filter design problem explained in Section 4.2. In that case, the chosen  $\epsilon_{th}$  is 0.007125, which corresponds to 143 nonzero values in the impulse response. The value  $E$  was 7.095%, and  $E_{opt}$  was 0.1364, which had an initial value of 0.08795. To have the same amount of side-lobes as the passband ripple, the passband and the stopband weights are taken as 1.

#### 4. Full-Wave Electromagnetic Simulation Results

Full-wave electromagnetic simulations, conducted in CST Microwave Studio<sup>®</sup> (CST-MWS) (Release Version 2020.01) for a ULA of 15 broadband antipodal Vivaldi antennas, are used to obtain the far-field transmit beam patterns produced by the proposed transmit beamformer. Here, we consider both multibeam and single-beam beamforming. The transmit signal frequency range of interest is  $[f_L = 1.3, f_H = 2.8]$  GHz, which has a fractional bandwidth of more than  $B_f = 70\%$ . The ULA of Vivaldi antennas is shown in Figure 6a, and the  $S_{11}$  curve of a single antenna element is shown in Figure 6b, verifying the wideband element response within the frequency range of interest. The interelement spacing is selected as  $\lambda/2$  such that  $\Delta x = \Delta ct$ , where  $\lambda$  is the wavelength corresponding to the temporal sampling frequency  $F_s = 6$  GHz. The passband of the 2-D FIR trapezoidal filter is taken such that its temporal frequency is in this frequency range of interest, i.e.,  $[0.43\pi, 0.93\pi]$  rad/sample. The order and the maximum transition band of the filter, and other parameters of the trapezoid which vary with different cases of beamforming are mentioned in the corresponding places in Sections 4.1 and 4.2. These include angles  $\alpha_i \in [-45^\circ, 45^\circ]$ ,  $i = 1, 2, \dots, K$  and the half-angle  $\delta_k$  with respect to Figure 4. Matlab<sup>®</sup> (Version R2018a) software is used for generating the impulse response of the desired 2-D sparse FIR filter responsible for beamforming with the help of the CVX optimization toolbox and SeDuMi solver. It is then exported and fed into CST-MWS ULA model as port excitation signals for each antenna. To obtain the far-field transmit beam patterns in CST-MWS, far-field monitors are placed within the frequency range of interest. Transmit beam patterns produced by both the sparse and nonsparse 2-D FIR filters are then obtained and compared. For the single-beam case, the results of the proposed method are compared with similar approaches adapted from [32,39–41] such that the filters have the same specifications. In particular, we present the average of the DODs, their standard deviation (SD), average gain, and side-lobe levels in the passband frequency range 1.3–2.8 GHz. Side-lobe levels are considered in the range  $\theta \in [-90^\circ, 90^\circ]$ , and the peak and average side-lobe levels at a particular temporal frequency are computed with respect to the average gain of the main beams. Additionally, 2-D FIR filter performance in terms of the passband ripple and the stopband attenuation, and the DSP adder and multiplier complexity are presented.

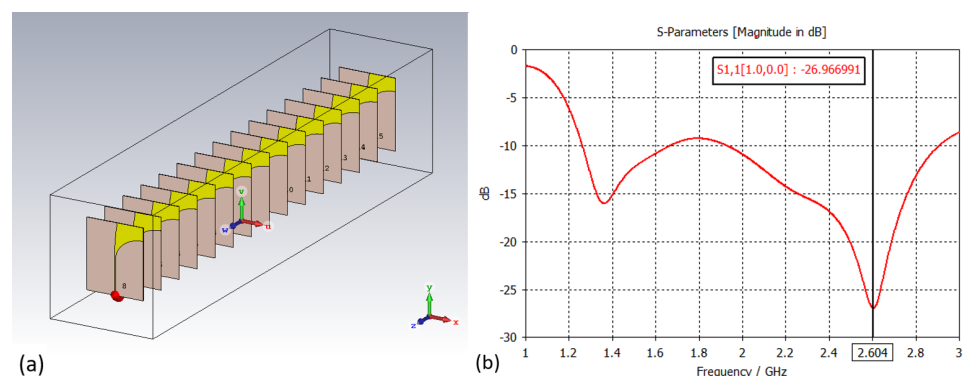


**Figure 6.** (a) ULA of 15-element antipodal Vivaldi antennas with an interelement spacing of 50 mm; (b)  $|S_{11}|$  plot of single antenna element made of Rogers RO4003 dielectric (dielectric constant: 3.55).

### 4.1. Multibeam Beamforming

Here, beamforming is achieved in  $K \in \mathbb{Z}^+$  directions, where  $K \geq 2$ . The DODs are  $\theta_i \in [-90^\circ, 90^\circ]$ ,  $i = 1, 2, \dots, K$ . Results for different independent signal transmissions (i.e., MSMB mode) and the same signal transmissions in different desired directions (i.e., SSMB mode) are discussed below. In the following examples, all the trapezoidal filters' half-angles  $\delta_k$  are taken as  $3^\circ$  and their maximum transition band is  $0.1\pi$  rad/sample. The region  $[-\pi, \pi] \times [0, \pi]$  in the 2-D frequency domain  $(\omega_x, \omega_{ct})$  is uniformly discretized into  $201 \times 101$  points. The passband and stopband weights are taken as 1.

#### 4.1.1. Two Independent Signals Transmission in Two DODs

As an example of two-direction beamforming where two independent signals are to be transmitted in different directions, consider the case where  $\theta_1 = -26^\circ$  and  $\theta_2 = 28^\circ$  with corresponding  $\alpha_1 = -23.67^\circ$  and  $\alpha_2 = 25.15^\circ$ , respectively. The magnitude frequency response  $|H(e^{j\omega_x}, e^{j\omega_{ct}})|$  of the sum of 2-D FIR filters of order  $14 \times 64$ , with nonspare impulse responses and with sparse impulse responses, is shown in Figure 7a and Figure 7b, respectively. Values for the other parameters are  $\mu = 0.05$  and  $\epsilon_{th} = 0.004997$  for DOD =  $-26^\circ$  filter and  $\mu = 0.05$  and  $\epsilon_{th} = 0.007005$  for DOD =  $28^\circ$  filter. The wideband transmit beam patterns produced by the nonspare filter and the proposed sparse filter outputs are shown in Figure 7e and Figure 7f, respectively. Furthermore, Table 1 provides a comparison of the wideband beam pattern and DSP complexity between the proposed 2D sparse and nonspare FIR filter-based transmit beamformers. The effect of sparsification is minimal on the passband ripple and side-lobe levels, while saving more than 85% in DSP complexity.

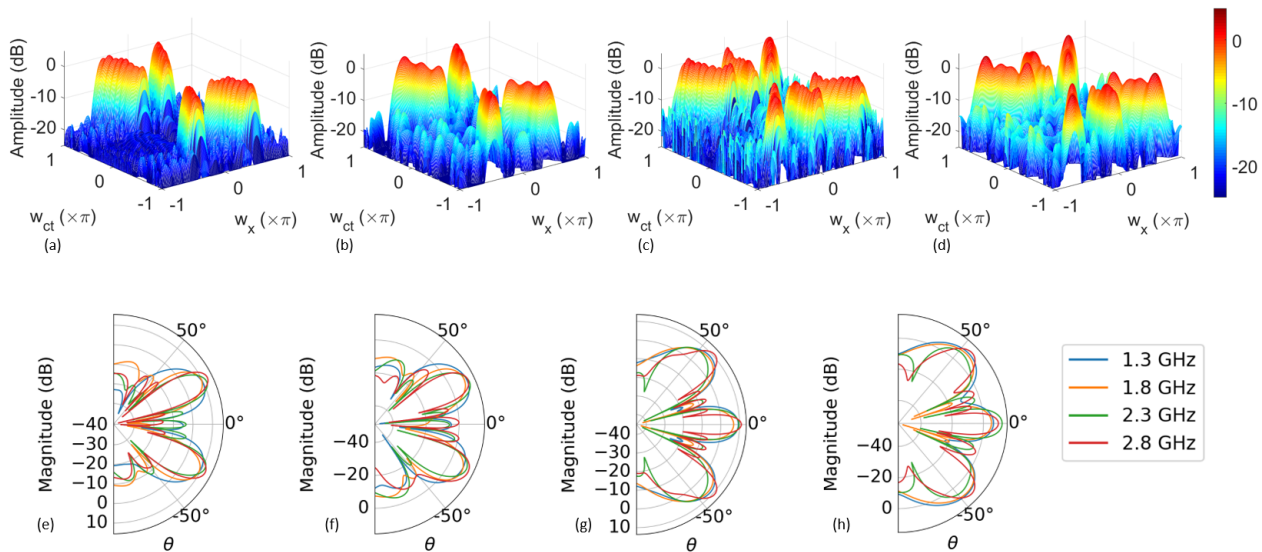


**Figure 7.** Magnitude frequency responses of the sum of 2D FIR filters  $|H(e^{j\omega_x}, e^{j\omega_{ct}})|$  designed for multiple independent signals transmission for DODs (a)  $(-28^\circ, 26^\circ)$  (non-sparse filter), (b)  $(-28^\circ, 26^\circ)$  (sparse filter), (c)  $(-45^\circ, 0^\circ, 45^\circ)$  (non-sparse filter), (d)  $(-45^\circ, 0^\circ, 45^\circ)$  (sparse filter). Polar plots of the simulated beam patterns obtained using the designed filters for DODs, (e)  $(-28^\circ, 26^\circ)$  (non-sparse filter), (f)  $(-28^\circ, 26^\circ)$  (sparse filter), (g)  $(-45^\circ, 0^\circ, 45^\circ)$  (non-sparse filter), and (h)  $(-45^\circ, 0^\circ, 45^\circ)$  (sparse filter).

**Table 1.** Accuracy of the beam pattern and the DSP complexity of the proposed sparse transmit beamformer and a nonsparse counterpart for the MSMB mode.

Case	$(-28^\circ, 26^\circ)$ DOD (Nonsparse FIR)		$(-28^\circ, 26^\circ)$ DOD (Sparse FIR)		$(-45^\circ, 0^\circ, 45^\circ)$ DOD (Nonsparse FIR)			$(-45^\circ, 0^\circ, 45^\circ)$ DOD (Sparse FIR)		
DOD (degrees)										
Average	-28.2	26.0	-27.3	25.9	-45.0	0.0	44.9	-45.6	0.0	45.6
Standard deviation	1.32	1.01	0.99	0.94	3.06	0.00	3.04	2.52	0.12	2.52
Gain (dB)										
Average	10.44	10.56	10.28	10.47	8.25	8.52	8.29	7.77	8.37	7.99
Side-lobe level † (dB)										
Peak	-17.18		-13.83		-17.76			-16.54		
Average	-26.11		-23.86		-22.28			-23.11		
Filter passband ripple (dB)										
Along main beam directions	2.25	2.07	2.34	2.84	3.32	3.10	3.32	4.00	3.61	4.54
In the defined passband		3.16		4.75		4.89			6.34	
Filter stopband attenuation (dB)										
Average in the defined stopbands	-28.86		-24.66		-25.80			-23.36		
DSP complexity										
AADs	974 + 974 = 1948		148 + 138 = 286		974 + 974 + 974 = 2922			120 + 164 + 120 = 404		
MULs	488 + 488 = 976		75 + 70 = 145		488 + 488 + 488 = 1464			61 + 83 + 61 = 205		

† with respect to the average gain.

### 4.1.2. Three Independent Signals Transmission in Three DODs

As an example of three-direction beamforming with three independent signals, consider the case where  $\theta_1 = -45^\circ$ ,  $\theta_2 = 0^\circ$ , and  $\theta_3 = 45^\circ$ , with corresponding  $\alpha_1 = -35.26^\circ$ ,  $\alpha_2 = 0^\circ$ , and  $\alpha_3 = 35.26^\circ$ , respectively. The magnitude frequency response  $|H(e^{j\omega_x}, e^{j\omega_{ct}})|$  of the sum of 2-D FIR filters of order  $14 \times 64$ , with nonsparse and with sparse impulse responses, is shown in Figure 8c and Figure 8d, respectively. Values for the other parameters are  $\mu = 0.05$  and  $\epsilon_{th} = 0.006998$  for DOD =  $\pm 45^\circ$  filters and  $\mu = 0.15$  and  $\epsilon_{th} = 0.006094$  for DOD =  $0^\circ$  filter. The wideband beam patterns produced by the nonsparse and sparse filters are shown in Figure 7g and Figure 7h, respectively. Moreover, Table 1 provides a comparison of wideband beam pattern and DSP complexity between the proposed 2D sparse and nonsparse FIR filter-based transmit beamformers. The results clearly indicate the minimal effect of sparsification of the filter impulse response towards the performance of the filter with regard to beamforming, saving more than 86% in DSP complexity.

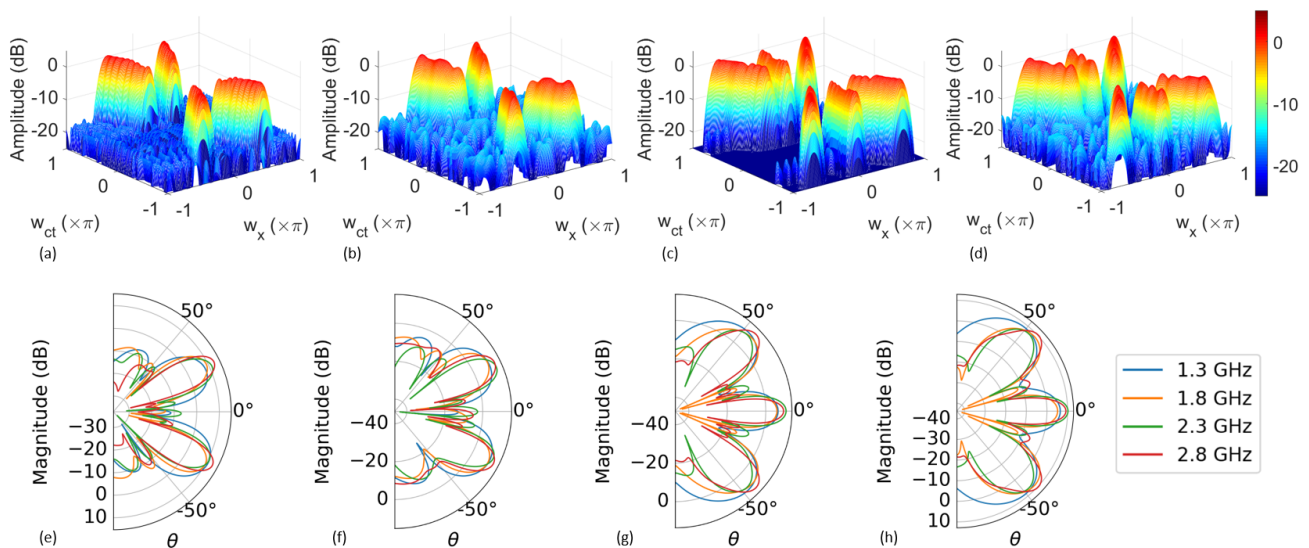


**Figure 8.** Magnitude frequency response of the 2-D FIR filters  $|H(e^{j\omega_x}, e^{j\omega_{ct}})|$  designed for the same signal transmission using the proposed method for DODs (a)  $(-28^\circ, 26^\circ)$  (nonsparse filter), (b)  $(-28^\circ, 26^\circ)$  (sparse filter), (c)  $(-45^\circ, 0^\circ, 45^\circ)$  (nonsparse filter), (d)  $(-45^\circ, 0^\circ, 45^\circ)$  (sparse filter). Polar plots of the simulated beam patterns obtained using the designed filter for DODs, (e)  $(-28^\circ, 26^\circ)$  (nonsparse filter), (f)  $(-28^\circ, 26^\circ)$  (sparse filter), (g)  $(-45^\circ, 0^\circ, 45^\circ)$  (nonsparse filter), and (h)  $(-45^\circ, 0^\circ, 45^\circ)$  (sparse filter).

#### 4.1.3. Same Signal Transmission in Two DODs

As an example of two-direction beamforming of the same signal, consider the case where  $\theta_1 = -26^\circ$  and  $\theta_2 = 28^\circ$ , with corresponding  $\alpha_1 = -23.67^\circ$  and  $\alpha_2 = 25.15^\circ$ , respectively. The magnitude frequency response  $|H(e^{j\omega_x}, e^{j\omega_{ct}})|$  of the 2-D FIR filters of order  $14 \times 64$ , with a nonsparse impulse response and sparse impulse response (with only 161 nonzero elements), is shown in Figure 8a and Figure 8b, respectively. Values for the other parameters are  $\mu = 0.1$  and  $\epsilon_{th} = 0.00701$ . The wideband transmit beam patterns produced by the nonsparse and sparse filters are shown in Figure 8e and Figure 8f, respectively. Furthermore, Table 2 provides a comparison of the wideband beam pattern and DSP complexity between the proposed 2D sparse and a nonsparse FIR filter-based transmit beamformers. We note that the effect of sparsification is minimal, while saving more than 83% in DSP complexity.

**Table 2.** Accuracy of the beam pattern and the DSP complexity of the proposed sparse transmit beamformer and a nonsparse counterpart for the SSMB mode.

Case	( $-28^\circ, 26^\circ$ ) DOD (Nonsparse FIR)		( $-28^\circ, 26^\circ$ ) DOD (Sparse FIR)		( $-45^\circ, 0^\circ, 45^\circ$ ) DOD (Nonsparse FIR)			( $-45^\circ, 0^\circ, 45^\circ$ ) DOD (Sparse FIR)		
	DOD (degrees)									
Average	-28.8	26.4	-27.9	26.4	-44.9	0.0	44.9	-45.5	0.0	45.4
Standard deviation	1.17	1.03	1.23	1.46	2.28	0.00	2.24	2.22	0.00	2.21
Gain (dB)										
Average	10.57	10.43	10.48	10.36	8.40	8.24	8.44	8.18	8.28	8.22
Side-lobe level <sup>†</sup> (dB)										
Peak		-17.67		-15.14					-18.39	
Average		-23.76		-22.25					-25.11	
Filter passband ripple (dB)										
Along main beam directions	1.84	2.98	2.64	2.61	1.23	2.21	1.23	1.90	2.81	1.90
In the defined passband		4.00		3.87		3.39			4.04	
Filter stopband attenuation (dB)										
Average in the defined stopband		-25.57		-24.17					-24.42	
DSP complexity										
ADDs		974		160		974			160	
MULs		488		81		488			81	

<sup>†</sup> with respect to the average gain.

#### 4.1.4. Same Signal Transmission in Three DODs

As an example of three-direction beamforming, consider the case where  $\theta_1 = -45^\circ$ ,  $\theta_2 = 0^\circ$ , and  $\theta_3 = 45^\circ$ , with corresponding  $\alpha_1 = -35.26^\circ$ ,  $\alpha_2 = 0^\circ$ , and  $\alpha_3 = 35.26^\circ$ , respectively. The magnitude frequency response  $|H(e^{j\omega_x}, e^{j\omega_{ct}})|$  of the 2-D FIR filters of order  $14 \times 64$ , with a nonsparse impulse response and a sparse impulse response (only with 161 nonzero elements), is shown in Figure 8c and Figure 8d, respectively. Values for the other parameters are  $\mu = 0.02$  and  $\epsilon_{th} = 0.010455$ . The wideband transmit beam patterns produced by the nonsparse and sparse filters are shown in Figure 8g and Figure 8h, respectively. Moreover, Table 2 provides a comparison of wideband beam pattern and DSP complexity between the proposed 2D sparse and nonsparse FIR filter-based transmit beamformers. The results clearly indicate the minimal effect of sparsification of the filter impulse response towards the performance of the filter with regard to beamforming, while saving more than 83% in DSP complexity.

#### 4.2. Single-Beam Beamforming

Here, beamforming is achieved in a single direction, where the DOD is  $\theta \in [-90^\circ, 90^\circ]$ . As an example of single-direction beamforming, consider the case where the DOD is  $30^\circ$ , where  $\alpha = 26.57^\circ$ . We design 2-D FIR trapezoidal filters using the windowing method and optimization techniques with nonsparse and sparse impulse responses. Here, the design of the filter with the windowing technique is adapted from [39,40] for the nonsparse impulse response whereas from [32] for the sparse impulse response. Furthermore, nonsparse filter designed using the optimization technique is adapted from [41] (without considering the mutual-coupling compensation for fair evaluation). For the windowing technique, the Dolph–Chebyshev window is used as the window function, because a Dolph–Chebyshev

window provides an approximately equiripple frequency magnitude response ([55], Chapter 9.4), and therefore an approximately minimax design. Furthermore, for the sparse impulse response [32], hard thresholding with a threshold of  $2.544 \times 10^{-4}$  is employed. The order of all of the filters is selected as  $14 \times 64$ , and the half-angle of the trapezoidal filter  $\delta$  is selected as  $3^\circ$ . Furthermore, the maximum transition band is  $0.1\pi$  rad/sample. The proposed filter is designed with the parameters  $\mu = 0.05$  and  $\epsilon_{th} = 0.007144$ . Furthermore, the passband and stopband weights are taken as 1, and the region  $[-\pi, \pi] \times [0, \pi]$  in the 2-D frequency domain  $(\omega_x, \omega_{ct})$  is uniformly discretized into  $201 \times 101$  points. The 2-D sparse FIR filters, i.e., those proposed and designed adapting the method in [41], have only 143 nonzero coefficients, whereas nonsparse filters have 975 coefficients. The magnitude frequency responses of the designed filters are shown in Figure 9a–d. Furthermore, Table 3 provides a comparison of the accuracy of the wideband beam patterns and DSP complexity for the proposed transmit beamformer and previously proposed filter designs. We observe that a significant reduction (more than 8 dB) in the passband ripple can be with the proposed transmit beamformer with similar stopband attenuation compared with the nonsparse [39,40] and sparse [32] filter designs based on the windowing technique. Furthermore, the average side-lobe level of the proposed beamformer is lower than 7 dB, and the peak side-lobe level is lower than 4 dB compared with these filters. Compared with the nonsparse optimization-based design [41], the proposed transmit beamformer provides a more than 85% reduction in DSP complexity without substantial degradation of the accuracy of the beam pattern. This confirms the superior performance of the proposed transmit beamformer compared with the transmit beamformers that employ 2-D FIR filters designed using previously proposed techniques [32,39–41].

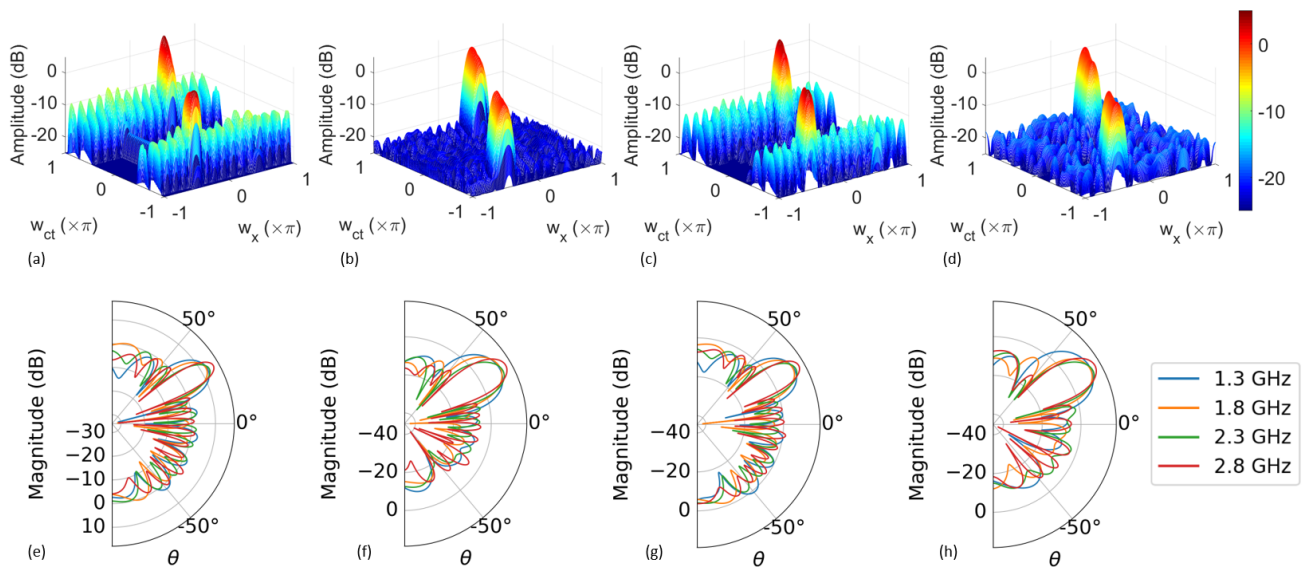


**Figure 9.** Magnitude frequency response of the 2D FIR trapezoidal filter  $|H(e^{j\omega_x}, e^{j\omega_{ct}})|$  for DOD =  $30^\circ$  using (a) windowing method [39,40] (nonsparse), (b) optimization (nonsparse) [41] (c) windowing method [32] (sparse), and (d) proposed (sparse). Polar plots of the simulated beam patterns obtained using the filter made using (e) windowing method [39,40] (nonsparse), (f) optimization [41] (nonsparse), (g) windowing method [32] (sparse), and (h) proposed (sparse).

**Table 3.** Accuracy of the beam pattern and the DSP complexity of the proposed sparse transmit beamformer and the single-beam sparse transmit beamformer designed using the windowing method [32] for the DOD = 30°.

Case	Windowing Method (Nonsparse FIR) [39,40]	Optimization (Nonsparse FIR) [41]	Windowing Method (Sparse FIR) [32]	Proposed (Sparse FIR)
DOD (degrees)				
Average	30.1	30.1	30.1	30.0
Standard deviation	0.33	0.87	0.39	0.85
Gain (dB)				
Average	13.43	13.43	13.67	13.30
Side-lobe level † (dB)				
Peak	−11.47	−20.75	−13.63	−17.96
Average	−17.02	−27.93	−19.76	−27.07
Filter passband ripple (dB)				
Along main beam directions	11.53	2.24	11.08	2.56
In the defined passband	12.81	2.87	11.81	3.28
Filter stopband attenuation (dB)				
Average in the defined stopband	−27.82	−28.94	−27.04	−27.32
DSP complexity				
ADDs	974	974	142	142
MULs	488	488	72	72

† with respect to the average gain.

## 5. Conclusions and Future Work

We propose a digitally fed wideband transmit multibeam beamformer using low-complexity 2-D sparse FIR trapezoidal filters with multiple trapezoidal passbands. The 2-D sparse FIR trapezoidal filter transforms a given wideband temporal input signal into a 2-D spatiotemporal signal with appropriate delays so that directional transmission can be achieved with a ULA of wideband antennas. We adapt a two-step sparse filter design method to design the 2-D sparse FIR trapezoidal filter optimal in the minimax sense. Full-wave electromagnetic simulations verify accurate wideband transmit beam patterns with more than 70% fractional bandwidth. More importantly, our 2-D sparse FIR trapezoidal filter provides significantly lower computational complexity compared with nonsparse counterparts. Furthermore, the proposed beamformer provides significantly better beam patterns for single-beam beamforming compared with the previously proposed sparse beamformer designed using the windowing method. Future work may include an extension of the proposed transmit beamformer to planar and other array geometries, implementations using analog-domain multidimensional filters, and experimental validation.

**Author Contributions:** Conceptualization, N.D., C.U.S.E., C.W. and A.M.; methodology, N.D. and C.U.S.E.; software, N.D.; validation, N.D., C.U.S.E., C.W. and A.M.; formal analysis, N.D., C.U.S.E., C.W. and A.M.; investigation, N.D., C.U.S.E., C.W. and A.M.; resources, N.D. and C.U.S.E.; data curation, N.D.; writing—original draft preparation, N.D., C.U.S.E. and A.M.; writing—review and editing, N.D., C.U.S.E., C.W. and A.M.; visualization, N.D.; supervision, C.U.S.E., C.W. and A.M.; project administration, C.U.S.E. and A.M.; funding acquisition, C.U.S.E. and A.M. All authors have read and agreed to the published version of the manuscript.

**Funding:** This research was partly supported by National Science Foundation (NSF), USA under the grant NSF SWIFT 2229471 and Senate Research Committee, University of Mortuwa under the grant SRC/LT/2020/08.

**Data Availability Statement:** The original contributions presented in the study are included in the article, further inquiries can be directed to the corresponding authors.

**Conflicts of Interest:** The authors declare no conflict of interest.

## References

1. Marzetta, T.L.; Larsson, E.G.; Yang, H.; Ngo, H.Q. *Fundamentals of Massive MIMO*; Cambridge University Press: New York, NY, USA, 2016.
2. Rappaport, T.S.; Xing, Y.; Kanhere, O.; Ju, S.; Madanayake, A.; Mandal, S.; Alkhateeb, A.; Trichopoulos, G.C. Wireless communications and applications above 100 GHz: Opportunities and challenges for 6G and beyond. *IEEE Access* **2019**, *7*, 78729–78757. [[CrossRef](#)]

3. Björnson, E.; Chae, C.B.; Heath, R.W., Jr.; Marzetta, T.L.; Mezghani, A.; Sanguinetti, L.; Rusek, F.; Castellanos, M.R.; Jun, D.; Demir, Ö.T. Towards 6G MIMO: Massive Spatial Multiplexing, Dense Arrays, and Interplay Between Electromagnetics and Processing. *arXiv* **2024**, arXiv:2401.02844.
4. Liu, Y.; Ouyang, C.; Ding, Z.; Schober, R. The Road to Next-Generation Multiple Access: A 50-Year Tutorial Review. *arXiv* **2024**, arXiv:2403.00189.
5. Haykin, S. *Array Signal Processing*; Prentice-Hall: Englewood Cliffs, NJ, USA, 1985.
6. Van Trees, H.L. *Optimum Array Processing*; John Wiley & Sons: New York, NY, USA, 2004.
7. Benesty, J.; Chen, J.; Huang, Y. *Microphone Array Signal Processing*; Springer: Berlin, Germany, 2008.
8. Liu, W.; Weiss, S. *Wideband Beamforming: Concepts and Techniques*; John Wiley & Sons: Chichester, UK, 2010.
9. Friedlander, B. On Transmit Beamforming for MIMO Radar. *IEEE Trans. Aerosp. Electron. Syst.* **2012**, *48*, 3376–3388. [[CrossRef](#)]
10. Rappaport, T.S.; Xing, Y.; MacCartney, G.R.; Molisch, A.F.; Mellios, E.; Zhang, J. Overview of Millimeter Wave Communications for Fifth-Generation (5G) Wireless Networks-With a Focus on Propagation Models. *IEEE Trans. Antennas Propag.* **2017**, *65*, 6213–6230. [[CrossRef](#)]
11. Boccardi, F.; Heath, R.W.; Lozano, A.; Marzetta, T.L.; Popovski, P. Five disruptive technology directions for 5G. *IEEE Commun. Mag.* **2014**, *52*, 74–80. [[CrossRef](#)]
12. Qamar, F.; Siddiqui, M.U.A.; Hindia, M.N.; Hassan, R.; Nguyen, Q.N. Issues, challenges, and research trends in spectrum management: A comprehensive overview and new vision for designing 6G networks. *Electronics* **2020**, *9*, 1416. [[CrossRef](#)]
13. Wang, W.; Gao, L.; Ding, R.; Lei, J.; You, L.; Chan, C.A.; Gao, X. Resource efficiency optimization for robust beamforming in multi-beam satellite communications. *IEEE Trans. Veh. Technol.* **2021**, *70*, 6958–6968. [[CrossRef](#)]
14. Gao, L.; Ma, J.; You, L.; Pan, C.; Wang, W.; Gao, X. Robust energy-efficient multigroup multicast beamforming for multi-beam satellite communications. In Proceedings of the ICC 2020-2020 IEEE International Conference on Communications (ICC), Dublin, Ireland, 7–11 June 2020; pp. 1–6.
15. Zhang, X.; Wang, J.; Jiang, C.; Yan, C.; Ren, Y.; Hanzo, L. Robust beamforming for multibeam satellite communication in the face of phase perturbations. *IEEE Trans. Veh. Technol.* **2019**, *68*, 3043–3047. [[CrossRef](#)]
16. Yu, L.; Wan, J.; Zhang, K.; Teng, F.; Lei, L.; Liu, Y. Spaceborne Multibeam Phased Array Antennas for Satellite Communications. *IEEE Aerosp. Electron. Syst. Mag.* **2023**, *38*, 28–47. [[CrossRef](#)]
17. Lin, Z.; An, K.; Niu, H.; Hu, Y.; Chatzinotas, S.; Zheng, G.; Wang, J. SLNR-Based Secure Energy Efficient Beamforming in Multibeam Satellite Systems. *IEEE Trans. Aerosp. Electron. Syst.* **2023**, *59*, 2085–2088. [[CrossRef](#)]
18. Xv, H.; Sun, Y.; Zhao, Y.; Peng, M.; Zhang, S. Joint Beam Scheduling and Beamforming Design for Cooperative Positioning in Multi-beam LEO Satellite Networks. *IEEE Trans. Veh. Technol.* **2023**, *73*, 5276–5287. [[CrossRef](#)]
19. Marzetta, T.; Yang, H. Massive MIMO in Line-of-Sight Propagation. In Proceedings of the 2017 IEEE 85th Vehicular Technology Conference (VTC Spring), Sydney, Australia, 4–7 June 2017.
20. Rappaport, T.S.; Sun, S.; Mayzus, R.; Zhao, H.; Azar, Y.; Wang, K.; Wong, G.N.; Schulz, J.K.; Samimi, M.; Gutierrez, F. Millimeter Wave Mobile Communications for 5G Cellular: It Will Work! *IEEE Access* **2013**, *1*, 335–349. [[CrossRef](#)]
21. Gong, S.; Lu, X.; Hoang, D.T.; Niyato, D.; Shu, L.; Kim, D.I.; Liang, Y.C. Toward Smart Wireless Communications via Intelligent Reflecting Surfaces: A Contemporary Survey. *IEEE Commun. Surv. Tutorials* **2020**, *22*, 2283–2314. [[CrossRef](#)]
22. Liu, Y.; Liu, X.; Mu, X.; Hou, T.; Xu, J.; Di Renzo, M.; Al-Dhahir, N. Reconfigurable intelligent surfaces: Principles and opportunities. *IEEE Commun. Surv. Tutorials* **2021**, *23*, 1546–1577. [[CrossRef](#)]
23. Yu, H.; Li, P.; Su, J.; Li, Z.; Xu, S.; Yang, F. Reconfigurable Bidirectional Beam-Steering Aperture With Transmitarray, Reflectarray, and Transmit-Reflect-Array Modes Switching. *IEEE Trans. Antennas Propag.* **2023**, *71*, 581–595. [[CrossRef](#)]
24. Han, S.; Chih-Lin, I.; Xu, Z.; Rowell, C. Large-scale antenna systems with hybrid analog and digital beamforming for millimeter wave 5G. *IEEE Commun. Mag.* **2015**, *53*, 186–194. [[CrossRef](#)]
25. Ioushua, S.S.; Eldar, Y.C. A family of hybrid analog–digital beamforming methods for massive MIMO systems. *IEEE Trans. Signal Process.* **2019**, *67*, 3243–3257. [[CrossRef](#)]
26. Slezak, C.; Dhananjay, A.; Rangan, S. 60 GHz blockage study using phased arrays. In Proceedings of the 2017 51st Asilomar Conference on Signals, Systems, and Computers, Pacific Grove, CA, USA, 29 October–1 November 2017; pp. 1655–1659. [[CrossRef](#)]
27. Dutta, S.; Barati, C.N.; Ramirez, D.; Dhananjay, A.; Buckwalter, J.F.; Rangan, S. A Case for Digital Beamforming at mmWave. *IEEE Trans. Wirel. Commun.* **2020**, *19*, 756–770. [[CrossRef](#)]
28. Dutta, S.; Barati, C.N.; Dhananjay, A.; Rangan, S. 5G millimeter wave cellular system capacity with fully digital beamforming. In Proceedings of the 2017 51st Asilomar Conference on Signals, Systems, and Computers, Pacific Grove, CA, USA, 29 October–1 November 2017; pp. 1224–1228. [[CrossRef](#)]
29. Madanayake, A.; Ariyaratna, V.; Madishetty, S.; Pulipati, S.; Cintra, R.J.; Coelho, D.; Oliviera, R.; Bayer, F.M.; Belostotski, L.; Mandal, S.; et al. Towards a Low-SWaP 1024-Beam Digital Array: A 32-Beam Subsystem at 5.8 GHz. *IEEE Trans. Antennas Propag.* **2020**, *68*, 900–912. [[CrossRef](#)]
30. Madanayake, A.; Cintra, R.J.; Akram, N.; Ariyaratna, V.; Mandal, S.; Coutinho, V.A.; Bayer, F.M.; Coelho, D.; Rappaport, T.S. Fast Radix-32 Approximate DFTs for 1024-Beam Digital RF Beamforming. *IEEE Access* **2020**, *8*, 96613–96627. [[CrossRef](#)]
31. Qi, Z.; Yunhao, L.; Ying, X.; Bin, T. Transmit Multi-beamforming of Wideband Signals Based on the Focusing Transform. In Proceedings of the 2014 IEEE 17th International Conference on Computational Science and Engineering, Chengdu, China, 19–21 December 2014; pp. 1043–1046.

32. Edussooriya, C.U.; Wijenayake, C.; Pulipati, S.; Madanayake, A.; Bruton, L.T. Low-Complexity Wideband Transmit Array using Variable-Precision 2-D Sparse FIR Digital Filters. In Proceedings of the 2019 IEEE International Symposium on Circuits and Systems (ISCAS), Sapporo, Japan, 26–29 May 2019; pp. 1–5.
33. Ba, H.C.; Shirai, H.; Ngoc, C.D. Analysis and design of antipodal Vivaldi antenna for UWB applications. In Proceedings of the 2014 IEEE Fifth International Conference on Communications and Electronics (ICCE), Danang, Vietnam, 30 July–1 August 2014; pp. 391–394. [\[CrossRef\]](#)
34. Neinhuis, M.; Solbach, K. Finite impulse response-filter-based RF-beamforming network for wideband and ultra-wideband antenna arrays. *IET Microw. Antennas Propag.* **2011**, *5*, 844–851. [\[CrossRef\]](#)
35. Gao, Y.; Jiang, D.; Liu, M. Wideband transmit beamforming using integer-time-delayed and phase-shifted waveforms. *Electron. Lett.* **2017**, *53*, 376–378. [\[CrossRef\]](#)
36. Uysal, F.; Dunn, Z. Application of waveform weighting for a frequency- invariant transmit beampattern. *IEEE Aerosp. Electron. Syst. Mag.* **2016**, *31*, 4–12. [\[CrossRef\]](#)
37. Sekiguchi, T.; Karasawa, Y. Wideband beamspace adaptive array utilizing FIR fan filters for multibeam forming. *IEEE Trans. Signal Process.* **2000**, *48*, 277–284. [\[CrossRef\]](#)
38. Nishikawa, K. Wideband multi-beam forming method using delayed array sensors and two-dimensional digital filter. *Electron. Commun. Jpn. Part 3* **2005**, *88*, 1–12. [\[CrossRef\]](#)
39. Gunaratne, T.K.; Bruton, L.T. Broadband beamforming of bandpass plane waves using 2D FIR trapezoidal filters at baseband. In Proceedings of the APCCAS 2006-2006 IEEE Asia Pacific Conference on Circuits and Systems, Singapore, 4–7 December 2006; pp. 546–549.
40. Gunaratne, T.K.; Bruton, L.T. Beamforming of Broad-Band Bandpass Plane Waves Using Polyphase 2-D FIR Trapezoidal Filters. *IEEE Trans. Circuits Syst. I* **2008**, *55*, 838–850. [\[CrossRef\]](#)
41. Pulipati, S.; Ariyaratna, V.; Jayaweera, A.L.; Edussooriya, C.U.S.; Wijenayake, C.; Belostotski, L.; Madanayake, A. FPGA-Based 2-D FIR Frost Beamformers with Digital Mutual Coupling Compensation. In Proceedings of the 2020 IEEE/MTT-S International Microwave Symposium (IMS), Los Angeles, CA, USA, 4–6 August 2020; pp. 1077–1080.
42. Pulipati, S.; Ariyaratna, V.; Madanayake, A.; Wijesekara, R.T.; Edussooriya, C.U.; Bruton, L.T. A 16-Element 2.4-GHz Multi-Beam Array Receiver using 2-D Spatially-Bandpass Digital Filters. *IEEE Trans. Aerosp. Electron. Syst.* **2019**, *55*, 3029–3038. [\[CrossRef\]](#)
43. Hong, W.; Jiang, Z.H.; Yu, C.; Zhou, J.; Chen, P.; Yu, Z.; Zhang, H.; Yang, B.; Pang, X.; Jiang, M.; et al. Multibeam Antenna Technologies for 5G Wireless Communications. *IEEE Trans. Antennas Propag.* **2017**, *65*, 6231–6249. [\[CrossRef\]](#)
44. Shen, D.; Dai, L.; Su, X.; Suo, S. Multi-Beam Design for Near-Field Extremely Large-Scale RIS-Aided Wireless Communications. *IEEE Trans. Green Commun. Netw.* **2023**, *7*, 1542–1553. [\[CrossRef\]](#)
45. Yan, J.; Liu, H.; Jiu, B.; Chen, B.; Liu, Z.; Bao, Z. Simultaneous Multibeam Resource Allocation Scheme for Multiple Target Tracking. *IEEE Trans. Signal Process.* **2015**, *63*, 3110–3122. [\[CrossRef\]](#)
46. Zhang, J.A.; Huang, X.; Guo, Y.J.; Yuan, J.; Heath, R.W. Multibeam for Joint Communication and Radar Sensing Using Steerable Analog Antenna Arrays. *IEEE Trans. Veh. Technol.* **2019**, *68*, 671–685. [\[CrossRef\]](#)
47. Sahin, C.; McCormick, P.M.; Metcalf, J.G.; Blunt, S.D. Power-Efficient Multi-Beam Phase-Attached Radar/Communications. In Proceedings of the 2019 IEEE Radar Conference (RadarConf), Boston, MA, USA, 22–26 April 2019; pp. 1–6. [\[CrossRef\]](#)
48. Monteys, X.; Harris, P.; Caloca, S.; Cahalane, C. Spatial prediction of coastal bathymetry based on multispectral satellite imagery and multibeam data. *Remote Sens.* **2015**, *7*, 13782–13806. [\[CrossRef\]](#)
49. Iupikov, O.A.; Ivashina, M.V.; Skou, N.; Cappellin, C.; Pontoppidan, K.; van’t Klooster, C.G.M. Multibeam Focal Plane Arrays With Digital Beamforming for High Precision Space-Borne Ocean Remote Sensing. *IEEE Trans. Antennas Propag.* **2018**, *66*, 737–748. [\[CrossRef\]](#)
50. Bruton, L.; Bartley, N. Three-dimensional image processing using the concept of network resonance. *IEEE Trans. Circuits Syst.* **1985**, *32*, 664–672. [\[CrossRef\]](#)
51. Madanayake, A.; Wijenayake, C.; Dansereau, D.G.; Gunaratne, T.K.; Bruton, L.T.; Williams, S.B. Multidimensional (MD) circuits and systems for emerging applications including cognitive radio, radio astronomy, robot vision and imaging. *IEEE Circuits Syst. Mag.* **2013**, *13*, 10–43. [\[CrossRef\]](#)
52. Lu, W.S.; Hinamoto, T. Two-dimensional digital filters with sparse coefficients. *Multidimens. Syst. Signal Process.* **2011**, *22*, 173–189. [\[CrossRef\]](#)
53. Dudgeon, D.E. *Multidimensional Digital Signal Processing*; Prentice-Hall: Engewood Cliffs, NJ, USA, 1983.
54. Jayaweera, S.S.; Edussooriya, C.U.S.; Wijenayake, C.; Agathoklis, P.; Bruton, L. Multi-Volumetric Refocusing of Light Fields. *IEEE Signal Process. Lett.* **2021**, *28*, 31–35. [\[CrossRef\]](#)
55. Antoniou, A. *Digital Signal Processing: Signals, Systems, and Filters*; McGraw-Hill: New York, NY, USA, 2006.

**Disclaimer/Publisher’s Note:** The statements, opinions and data contained in all publications are solely those of the individual author(s) and contributor(s) and not of MDPI and/or the editor(s). MDPI and/or the editor(s) disclaim responsibility for any injury to people or property resulting from any ideas, methods, instructions or products referred to in the content.